Optimizing HF Radar Siting for Surveillance and Remote Sensing in the Strait of Malacca

Stuart J. Anderson

***Abstract*—The deployment of a network of HF surface wave radar (HFSWR) systems is a complex task with many factors to be considered, particularly when the radars are expected to perform multiple roles. Failure to treat the siting problem with appropriate care could seriously degrade performance in one or more radar missions. In this paper, we describe a practical technique for HFSWR network design, based on a genetic algorithm adapted to multi-objective optimization, and demonstrate its efficacy in the context of a hypothetical two-radar system deployed in the Strait of Malacca, a major waterway along which many critical surveillance requirements have been identified. The results confirm that quite disparate criteria can be taken into account with this approach and support our claim that this methodology can be extended to higher dimensions where exhaustive search is completely out of the question.**

***Index Terms*—Current measurement, high-frequency surface wave radar (HFSWR), ship detection, Strait of Malacca.**

I. Introduction

HIGH-FREQUENCY surface wave radar (HFSWR) is a highly cost-effective remote sensing technology for measuring waves and currents, and monitoring the movements of ships and aircraft, at over-the-horizon ranges. To place this in a specific context, the prospective coverage of a representative radar is shown in Fig. 1 for a hypothetical radar located on Pulau Pinang in the Strait of Malacca. No other sensor technology possesses the same combination of over-the-horizon coverage, day–night operation, ability to detect non-cooperating targets, remote sensing of sea conditions, and low cost per unit area under surveillance. Nominal performance of two representative HFSWR systems is summarized in Table I.

While some HFSWR systems have been designed and deployed with a single mission in mind, it is increasingly recognized that the versatility of this technology supports a variety of applications. For instance, one might wish to detect and track shipping in the Strait of Malacca but also to measure surface currents so that risks of collision or grounding can be minimized and any transport of pollution predicted. In addition, information on sea state is of interest to the fishing industry, planning for offshore wave energy extraction, coastal development, port operation scheduling, search and rescue, tourism and recreational activities, so extraction and dissemination of environmental data would be welcomed by a wide range of user communities. Of course, these various applications will have relative priorities which vary with location, time of day and season, as will the radar's ability to accomplish them.

The spatial resolution and ultimate sensitivity of HFSWR is primarily a function of radar design, but performance in its various candidate roles is also dependent on a wide variety of geographical factors, lithospheric, oceanic, atmospheric, and ionospheric. These factors impact on the radar measurement process by mechanisms which are individually reasonably well understood, but the complexity of their combined influence makes the optimization of radar siting too difficult for closed-form solution. Accordingly, one must resort to numerical optimization techniques in a multidimensional parameter space if one is to deploy a radar to best advantage. Moreover, a single radar can measure only one component of the instantaneous velocity vector of a moving target. For detection and tracking of ships and aircraft, observing target motion over time removes this limitation and the full velocity vector can be estimated. In contrast, ambiguity persists when mapping ocean currents, so current-mapping HFSWR systems are generally deployed in pairs, viewing the area of concern from different directions. This greatly complicates the choice of radar sites, particularly as the pair of locations offering the best combined performance for current mapping seldom includes the site that would offer the best performance if only a single radar were to be deployed. A similar observation holds for the choice of sites for a single bistatic radar, that is, one in which the transmit and receive facilities are not collocated. Experience has shown that relying on intuition, simplistic modeling, or educated guesswork can result in very sub-optimum outcomes.

In the face of these considerations, the question "what is the optimum choice of sites for deploying N radars so that overall performance is maximized?" demands precise formulation if a meaningful answer is to be found. For situations where performance is measurable by a single scalar figure of merit, such as the probability of detection of a specified target, the problem can be addressed by conventional optimization techniques, as demonstrated by Anderson [5]. When there are multiple objectives, though, we must find some way of balancing the respective requirements and potential conflicts between different radar missions.

This paper describes an approach to this problem based on the concept of Pareto dominance and illustrates it with a hypothetical deployment allowing for two radars deployed in the Strait of Malacca. In keeping with the great majority of HFSWR systems, we shall assume here that the radars operate

Manuscript received February 13, 2012; revised May 30, 2012; accepted June 24, 2012. Date of publication August 21, 2012; date of current version February 21, 2013.

The author is with the ISR Division, Defense Science and Technology Organization, Edinburgh, SA 5111, Australia (e-mail: stuart.anderson@dsto.defence.gov.au).

Digital Object Identifier 10.1109/TGRS.2012.2207390

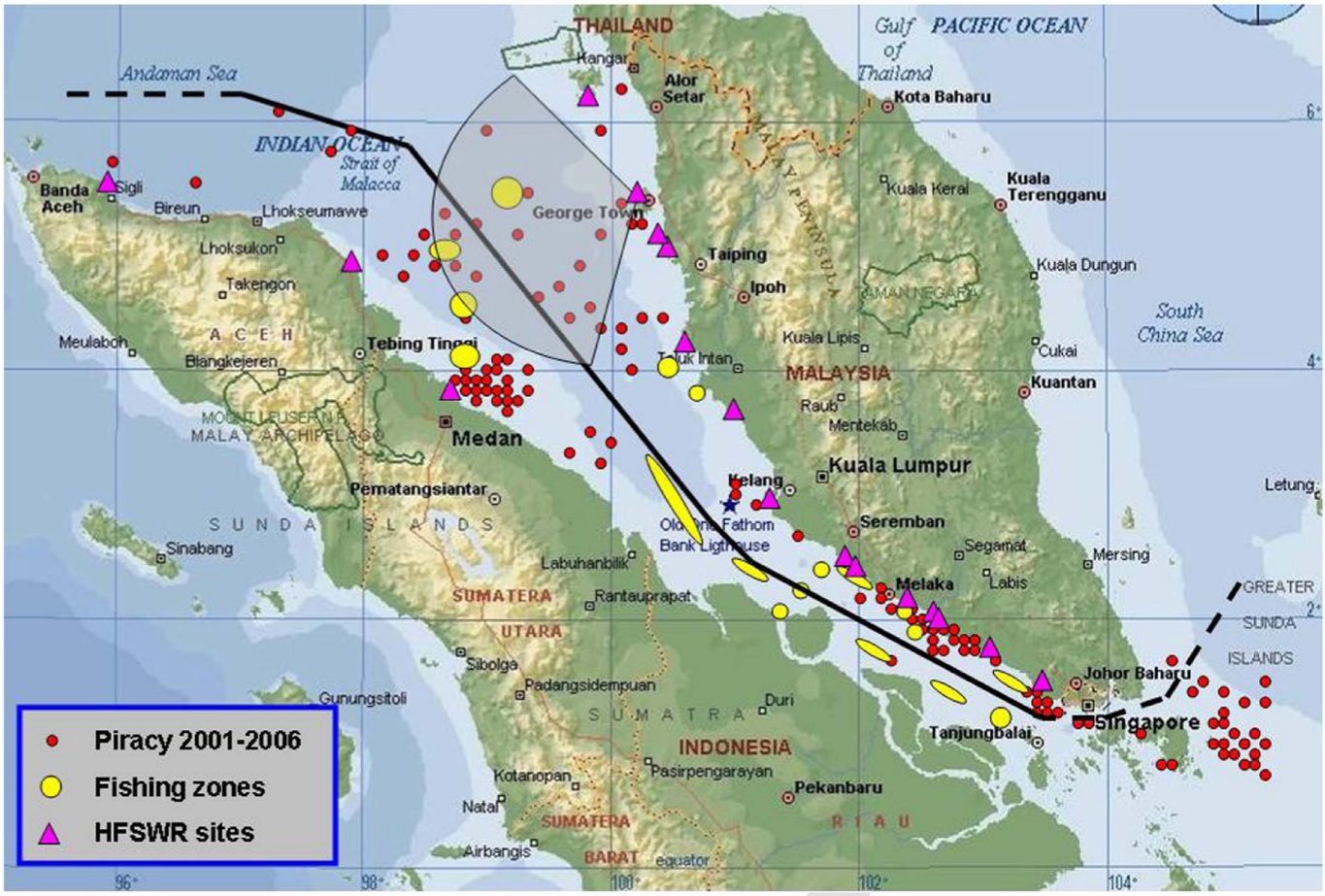

Fig. 1. Strait of Malacca, showing the main shipping lane, fishing zones, incidents of piracy, and the set of candidate HFSWR sites chosen as input to the optimization process. The nominal coverage of a single hypothetical radar located on Pulau Pinang is overlaid; the maximum range shown is 150 km.

TABLE I
NOMINAL PERFORMANCE OF REPRESENTATIVE HFSWR SYSTEMS AGAINST GENERIC MISSIONS. NOTE THAT COVERAGE AND ACCURACY ARE DEPENDENT ON SEA CONDITIONS, TARGET BEHAVIOR, AND OTHER FACTORS, A CONSIDERATION WHICH IS INDICATED HERE, BY CITING THE RANGE WITHIN WHICH EACH PARAMETER USUALLY LIES

Observable	Typical performance			
	low-cost civilian radar [1-3]		military radar [4]	
	max. range (km)	accuracy	max. range (km)	accuracy
surface current	60 - 200	± 0.02 – 0.20 m/s	350 - 450	± 0.02 – 0.10 m/s
wave height	30 - 100	± 10 – 25 %	150 - 250	± 10 – 20 %
wind direction	50 - 150	± 30° - 60°	320 - 400	± 20° - 30°
wind speed	30 - 100	± 20 %	200 - 250	± 20 %
large ship	50 - 180	± 0.5 - 3 km	300 - 450	± 0.5 – 3 km
fishing boat	20 - 65	± 0.5 – 2 km	120 - 280	± 0.5 – 2 km
small boat	10 - 25	± 0.5 – 1 km	70 - 150	± 0.5 – 1 km

in quasi-monostatic mode, that is the transmitting and receiving subsystems of each radar are located close together, and the exploitation of the other radar's transmissions in a bistatic scattering geometry is not pursued.

II. STRAIT OF MALACCA

Much of the world's economy rests on the safe and efficient flow of shipping through the waterway which separates Peninsular Malaysia, Thailand, and Singapore from the Indonesian island of Sumatera. As the main shipping channel between the Indian Ocean and the Pacific Ocean, via the Andaman Sea and the South China Sea, the Straits of Malacca and Singapore provide passage to over 40% of the world's traded goods. Some 15 million barrels of oil are transported through the Straits each day, providing 90% of Japan's imports and 80% of China's [6]. In 2008, more than 70 000 ships passed through the Straits to transport energy, raw materials, and finished goods. Over the past decade, shipping traffic has increased by more than 60%. Traffic density is projected to double by 2020.

This extreme concentration of shipping, in a narrow seaway with very shallow and changing bathymetry, numerous shoals, strong monsoonal winds in the northern reaches of the Strait, surface currents up to 5 knots [7] and a large, unregulated population of small fishing craft and local ship traffic makes for a very hazardous environment which has seen many accidents. On 15 October 1997, two oil tankers, the "ORAPIN GLOBAL" and the "EVOIKOS," collided in the Singapore Strait, causing the worst oil spill in the history of Singapore and East Asia. This collision resulted in about 28 500 tonnes of heavy marine fuel oil to be spilled into the sea [8]. Further, in addition to the navigational dangers of collision and grounding, piracy has historically been a serious problem in the Strait. In 2004, the Strait of Malacca was ranked as the world's most dangerous sea route, according to the International Maritime Bureau, with 38 attacks. After reaching an agreement to deal collectively with this issue, the governments of Malaysia, Singapore, and Indonesia instituted coordinated air and sea patrols, which significantly reduced attacks, to 11 in 2006 and only 2 in 2010, but with an upsurge in 2011 [9]–[11]. Needless to say, these patrols are expensive and can be defeated by pirates with access to intelligence. More recently, the prospect of acts of maritime terrorism has emerged as a grave threat [12], [13]. Fig. 1 shows the primary shipping channel, along with the locations of the main fishing zones and the areas with the highest incidence of piracy.

The Strait of Malacca is strongly influenced by the monsoons, with the north-east winds dominating during (northern) winter and the south-west winds in summer. Apart from their effects on the surface currents, they create distinctive wave spectra because of the fetch-limited development associated with the orientation of the Strait relative to the prevailing winds. From the radar perspective, this complicates the extraction of information from the measured clutter Doppler spectrum, necessitating the use of a sophisticated wave spectrum model [14].

III. Radar Siting and Configuration Design as a Multi-Objective Optimization Problem

A. Elements of the Formulation

At the outset, we can identify the data structures, procedures, and supporting information that need to be integrated into the problem formulation. These are:

(i) parameter space $\boldsymbol{P}$ in which the solutions must lie; here, we define $\boldsymbol{P}$ as the space of n-tuples of available locations, each belonging to the set of points $\boldsymbol{C}$ which comprise the coastline of Malaysia facing the Strait of Malacca;
(ii) the amenity of each coastal location to the installation of a radar, taking into account factors such as accessibility, power supply, field of view, and environmental impact;
(iii) the range and azimuthal coverage of the individual radars to be used, noting that the former is a function of the target radar cross section (RCS);
(iv) the wind, wave, and current climatology of the waters of the Strait of Malacca;
(v) the recognized shipping lanes;
(vi) the types of vessels of interest or, more specifically, their typical speeds and RCSs;
(vii) the surveillance and remote sensing missions assigned to the radar system and associated criteria which quantify performance;
(viii) algorithms which compute the radar response for any given combination of ship type, course, speed, and environmental conditions;
(ix) the objective function space $\boldsymbol{Y}$, i.e., the m-dimensional space whose coordinates measure the radar performance against the m tasks assigned to the radar;
(x) a search algorithm which finds the extrema of a scalar function over a specified domain;
(xi) a criterion for ranking solutions which achieve extrema in one or more coordinates of $\boldsymbol{Y}$.

It is common practice to formulate optimization problems in terms of minimizing the objective functions rather than maximizing them, which is trivially achieved by redefining the coordinates of $\boldsymbol{Y}$; we shall follow this practice.

With this palette of ingredients, the radar siting problem can be stated as follows: Find the n-tuple(s) of locations, $(\boldsymbol{r_1^{opt}}, \boldsymbol{r_2^{opt}}, \ldots \boldsymbol{r_n^{opt}})$ belonging to the design parameter space $\boldsymbol{X} \equiv \boldsymbol{C} \times \boldsymbol{C} \times \ldots \times \boldsymbol{C}$ which minimize(s) the m-vector $\boldsymbol{y}$ in the objective space $\boldsymbol{Y}$ under the action of the objective function mapping $\boldsymbol{\mu} : \boldsymbol{X} \rightarrow \boldsymbol{Y}$, i.e.,

$$\left(\boldsymbol{r_1^{opt}}, \boldsymbol{r_2^{opt}}, \ldots \boldsymbol{r_n^{opt}}\right) = \boldsymbol{min}_{\boldsymbol{x} \in \boldsymbol{X}} \left(\boldsymbol{\mu}(\boldsymbol{x})\right).$$

B. Multi-Objective Optimization Via Pareto Dominance

The definition of the problem given above is in one sense incomplete—it does not specify the choice of norm for the space $\boldsymbol{Y}$. In a single objective optimization problem, the objective space is usually a subset of the real numbers and a solution $\boldsymbol{x}_1 \in \boldsymbol{P}$ is better than another solution $\boldsymbol{x}_2 \in \boldsymbol{P}$ if $\boldsymbol{y}_1 < \boldsymbol{y}_2$ where $\boldsymbol{y}_1 = \boldsymbol{\mu}(\boldsymbol{x_1})$ and $\boldsymbol{y}_2 = \boldsymbol{\mu}(\boldsymbol{x_2})$. In the case of a vector-valued objective function mapping, comparing solutions is more complex, and one must endeavor to capture the essential priorities of the problem in the choice of norm. Herein lies the crucial distinction between single objective and multi-objective problems—whereas the former afford simple scalar measures of fitness that can be used to rank individual members of the design space, the latter are characterized by conflicts of interest among the competing objectives as measured by μ_i, $i = 1, m$.

There are several ways to deal with this complication. Perhaps, the simplest is to create a scalar figure of merit as a weighted sum of the separate objective measures,

(i) minimize $\mu^{(1)} = \sum_{i=1}^{m} \alpha_i \mu_i$.

Another approach is to convert all but one of the objectives into constraints,

(ii) minimize μ_j subject to $\mu_i \leq z_i \forall i = 1, m; i \neq j$.

While convenient, these methods shed little light on the nature of the tradeoffs made. As there may be subtle, non-quantifiable considerations involved in site selection, such as risks to personnel or to equipment, a better approach is to map the tradeoff surface so that the decision maker can execute

judgment in making a final selection. To perform this mapping, it is not necessary to run (i) or (ii) above for a large number of parameter selections α_i, z_i and to inspect the outcomes. Instead, we can use an evolutionary stochastic optimization algorithm to reveal the Pareto front, as described below.

Pareto optimality is based on the binary relation of dominance. A solution $\boldsymbol{x}_1 \in \boldsymbol{X}$ is said to be dominated by another solution $\boldsymbol{x}_2 \in \boldsymbol{X}$, written $\boldsymbol{x}_2 \prec \boldsymbol{x}_1$, if $\boldsymbol{x}_2$ is at least as good on all counts (objectives) and better on at least one, i.e.,

$$\boldsymbol{\mu}_i(\boldsymbol{x}_2) \leq \boldsymbol{\mu}_i(\boldsymbol{x}_1) \forall i = 1, m \text{ and } \boldsymbol{\mu}_j(\boldsymbol{x_2}) < \boldsymbol{\mu}_j(\boldsymbol{x_1}) \text{ for some } j.$$

With this relation, the Pareto set of optimal (non-dominated) solutions $\boldsymbol{P}^*$ will usually have multiple entries, associated with different tradeoffs between the objectives. The image $\boldsymbol{Y}^* \subset \boldsymbol{Y}$ of the Pareto set $\boldsymbol{P}^* \subset \boldsymbol{P}$ is referred to as the Pareto front, and knowledge of its shape greatly assists in choosing the best compromise solution.

C. Implementation via Genetic Algorithms

Classical techniques for finding extrema of functions defined on prescribed domains rely, in most cases, on gradient search methodologies. Such techniques are vulnerable to being trapped on local extrema, rather than the global extremum of main interest. In addition, the convergence may be slow, particularly near the extrema, necessitating the invocation of higher order derivatives. While there are ways to alleviate these weaknesses, they come at considerable cost. An alternative approach, now in widespread use, is to emulate evolutionary mechanisms which we observe in action in the natural world. The best known of these evolutionary optimization techniques are genetic algorithms.

Genetic algorithms encode the parameter values associated with each candidate solution as a string, usually in binary format. For each parameter, the number of bits provided must be sufficient to encode the full range of possible values associated with that parameter. The string representing a solution is simply the concatenation of the sub-strings corresponding to the individual parameters; by analogy with biology, this string is referred to as a chromosome. Starting with an initial population of candidate solutions (i.e., chromosomes) constructed by means of a random number generator, a genetic algorithm iteratively applies three basic steps: 1) rank the members of the current population according to fitness, 2) select superior members which will be used to breed the next generation, and 3) apply operators on randomly-selected pairs of these members to mimic the transfer of genetic material to offspring that occurs during biological reproduction, thereby producing a new generation with statistically superior characteristics.

In our implementation, the dominant transfer of information from one generation to the next is variable length cross-over. For each pair of chromosomes selected to breed together, the start and end indices of a sub-string are selected by a random number generator, and the corresponding sub-strings are exchanged. The excisions are not forced to align with the parameter sub-string boundaries. The offspring of this coupling have parts in common with each parent and in general will represent new solutions. A small fraction of this new set of chromosomes is then subjected to mutation, that is, one or two bits may be flipped to produce a different string, which of course maps onto a different candidate solution. This completes the process of constructing a new generation.

With single objective optimization, it is a simple matter to rank the members of the resulting population so that selection of candidates for constructing the next generation can proceed. Chromosomes representing the best solutions are carried over unchanged to the next generation, as well as participating in the breeding cycle, while the least fit are discarded. The resulting population is then allowed to breed in its turn, via cross-over and mutation. After passing through a large number of generations, the population tends to converge toward a uniform composition whose members share the most desirable parameter values. Importantly, by virtue of the randomness of the cross-over and mutation operations, candidate solutions from all over the solution domain are potentially represented, and mutation ensures that this property is maintained, so that the population is unlikely to be trapped on a local extremum if a superior solution exists.

With multi-objective optimization, the key objective is to find the Pareto front, but our experience is that coverage and convergence can be improved by relying on more than just Pareto dominance for selection. In our approach, each chromosome was tested against its contemporaries and those which were Pareto dominant were automatically selected, while those which had only one or two dominators were also short listed. In addition, members that performed particularly well against just one objective function were retained. Supplementing these criteria, a scalar figure of merit was defined by taking the product of the individual objective functions; this provided another metric for selection. The total size of the population was maintained at the initial value by allowing each of these different selection mechanisms to contribute a fraction of the membership, with the relative proportions changing with the generation index.

We modified the single objective genetic algorithm developed in [5], [15] to embody these ideas and hence to compute an estimate of the Pareto front. The radars were assumed to have identical design, each with a specified boresight and maximum range. As these parameters are not variable in our formulation, they do not need to be represented in the chromosome. In this situation, only the identities of the two radars need be encoded, so when 16 possible sites are available, the chromosome needs only eight bits, that is, four for the site of radar 1, four for the site of radar 2.

D. Constructing the Objective Function Space

To illustrate, we shall suppose that two tasks are of primary importance: 1) detection of ships, and 2) measurement of ocean currents which are perpendicular to the shipping lanes and hence could cause ships to collide or run aground. Suitable individual objective functions to be minimized can be constructed from spatial averages of figures of merit corresponding to the radar performance in the respective tasks, as will be shown below. The required figures of merit for networks of radars

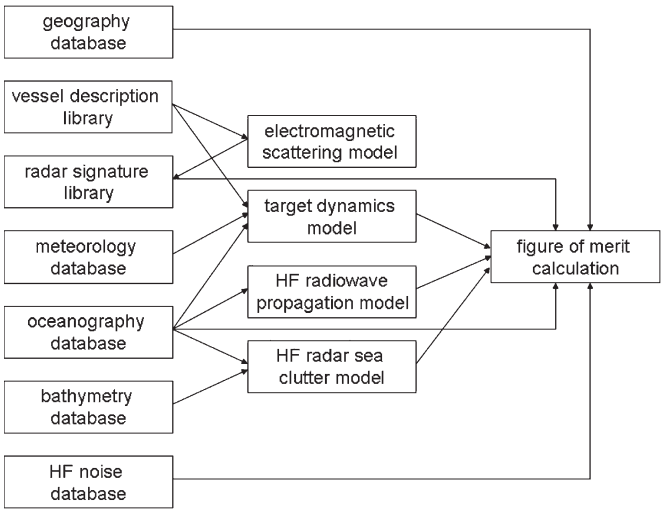

Fig. 2. Databases and physical models used to evaluate radar configurations.

are constructed via precursors which are defined for individual radars, which are then generalized. Central to the design of these and other figures of merit is access to the databases which describe the radar environment and the characteristics of the vessels of interest. A schematic showing how these are linked to the modules which compute the figures of merit is included below as Fig. 2.

1) Ship Detection: Suppose an HFSWR operating at a fixed center frequency f is deployed with the goal of detecting ships whose RCS exceeds some specified threshold. For detection, we require that a ship echo exceed the clutter and noise power in the same Doppler bin by some margin ε, that is, there exists $\omega \in [-\Omega, \Omega]$ such that $s(\omega) > c(\omega) + n(\omega) + \varepsilon$ where $s(\omega)$, $c(\omega)$ and $n(\omega)$ are the target, clutter, and noise power spectral densities, respectively, and $[-\Omega, \Omega]$ is the extent of the Doppler domain. For almost all situations of relevance to this application, the clutter power spectral density exceeds that of noise, so, with no real loss of generality, we shall ignore the noise term in what follows.

In the context of the Strait of Malacca, we may be concerned with two categories of shipping. The primary group consists of commercial vessels proceeding along known shipping lanes at fairly uniform speeds, $v \in [v_{min}, v_{max}]$ so the Doppler perceived by the radar from a given ship is a function of a single coordinate, representing the ship's position along its chosen lane, since that determines the viewing geometry. Accordingly, for these targets, it makes good sense to define a figure of merit which measures the fraction of the time (equivalently distance along the route under surveillance) for which such ships are detectable

$$FoM\_1 = \int_L max_{\omega \in Z} H(s(\omega;\boldsymbol{r}) - c(\omega;\boldsymbol{r}) - \varepsilon)\, d\boldsymbol{r} \times \left[\int_L d\boldsymbol{r}\right]^{-1} \tag{1}$$

where $H(x)$ is the Heaviside function

$$H(x) = \begin{matrix} 0 & x < 0 \\ 1 & x \geq 0. \end{matrix} \tag{2}$$

L signifies the portion of the shipping lane within the Strait of Malacca jurisdiction and

$$Z \triangleq \left[\frac{2v_{min}f}{c}, \frac{2v_{max}f}{c}\right]. \tag{3}$$

It is a computationally trivial but operationally useful generalization to apply a weighting according to the geographical position

$$FoM\_2 = \int_L w(\boldsymbol{r}) max_{\omega \in Z} H\left(s\left(\omega;\boldsymbol{r}\right) - c(\omega;\boldsymbol{r}) - \varepsilon\right) d\boldsymbol{r} \times \left[\int_L w(\boldsymbol{r}) d\boldsymbol{r}\right]^{-1} \tag{4}$$

which could reflect the distribution of navigation hazards, risk of piracy, cross-Strait traffic density and so on. To evaluate these integrals, we need expressions for $s(\omega;\boldsymbol{r})$ and $c(\omega;\boldsymbol{r})$. The former can be written

$$s(\omega;\boldsymbol{r}) = R(\psi_{Rx}) \left(\frac{c^2}{4\pi f^2}\right) G(\boldsymbol{r}_{Rx}, \boldsymbol{r}) \sigma(\varphi_{scat}, \varphi_{inc}) \times \delta(\omega - \omega_D) G(\boldsymbol{r}, \boldsymbol{r}_{Tx}) T(\psi_{Tx}) P_{Tx} \tag{5}$$

with P_{Tx} the transmitted power, $T(\psi_{Tx})$ and $R(\psi_{Rx})$ denoting the azimuthal gain patterns of the transmit and receive antennas, c the free-space velocity of light, $G(\boldsymbol{r}_2, \boldsymbol{r}_1)$ representing the propagation loss factor between positions $\boldsymbol{r}_1$ and $\boldsymbol{r}_2$, and $\sigma(\varphi_{scat}, \varphi_{inc})$ the bistatic RCS for an incident angle φ_{inc} and scattered angle φ_{scat} as defined at $\boldsymbol{r}$, and ω_D the Doppler shift associated with the target echo

$$\omega_D = \frac{-f}{c} \times \frac{d}{dt}\left(|\boldsymbol{r} - \boldsymbol{r}_{Tx}| + |\boldsymbol{r} - \boldsymbol{r}_{Rx}|\right). \tag{6}$$

For target-specific criteria, the RCS must be calculated using a computational electromagnetics code such as NEC4 or FEKO. We have chosen here to restrict attention to the monostatic case, so $\varphi_{scat} = \varphi_{inc}$.

The corresponding expression for $c(\omega;\boldsymbol{r})$ takes the form

$$c(\omega;\boldsymbol{r}) = R(\psi_{Rx}) \left(\frac{c^2}{4\pi f^2}\right) G(\boldsymbol{r}_{Rx}, \boldsymbol{r}) \sigma(\omega; \varphi_{scat}, \varphi_{inc}, \boldsymbol{r}) \times G(\boldsymbol{r}, \boldsymbol{r}_{Tx}) T(\psi_{Tx}) P_{Tx} A \tag{7}$$

Here, A denotes the area of the resolution cell, whose cross-range dimension increases with range from the receiver. The cell's range extent is determined, in general, by the bandwidth B of the transmitted waveform and, for a phased array system of aperture L_{Rx}, we can write

$$A \approx \frac{c^2 |\boldsymbol{r} - \boldsymbol{r}_{Rx}|}{2BL_{Rx} F cos\psi_{Rx}}. \tag{8}$$

The sea surface scattering coefficient $\sigma(\omega; \varphi_{scat}, \varphi_{inc}, \boldsymbol{r})$ has a continuum of spectral content and, being dependent on sea state, will normally vary with position. For monostatic

scattering, the well-known formula of Barrick (see e.g., [16]) can be employed

$$\sigma(\omega;\boldsymbol{r}) = 2^6\pi k_0^4 \Bigg[\sum_{m=\pm1} S(m\boldsymbol{\kappa};\boldsymbol{r})\delta(\omega - m\sqrt{g\kappa})\delta(\boldsymbol{\kappa}-2\boldsymbol{k}_0) + \sum_{m_1=\pm1}\sum_{m_2=\pm1}\iint \Gamma^2(m_1\boldsymbol{\kappa}_1, m_2\boldsymbol{\kappa}_2) \times S(m_1\boldsymbol{\kappa}_1;\boldsymbol{r})S(m_2\boldsymbol{\kappa}_2;\boldsymbol{r})\delta(\boldsymbol{\kappa}_1+\boldsymbol{\kappa}_2-2\boldsymbol{k}_0) \times \delta(\omega - m_1\sqrt{g\kappa_1} - m_2\sqrt{g\kappa_2})d\boldsymbol{\kappa}_1 d\boldsymbol{\kappa}_2 \Bigg] \quad (9)$$

where $S(\boldsymbol{\kappa};\boldsymbol{r})$ is the directional wave spectrum at location $\boldsymbol{r}$ and $\Gamma^2(m_1\boldsymbol{\kappa}_1, m_2\boldsymbol{\kappa}_2)$ is a kernel which contains, inter alia, the polarization dependence. If bistatic operations are supported, it becomes necessary to employ a more general solution [17].

For an operational deployment, one would compute figures of merit averaged over time of day and the seasons, for which we would need wind, wave, and current climatologies. If appropriate, a weighting factor could be applied to effect diurnal or seasonal priorities.

A second category of shipping includes local and cross-Strait traffic, not overlooking vessels which may be engaged in illegal activities such as smuggling and piracy. Few of these vessels report their positions via the automatic identification system mandated by the International Maritime Organization for vessels above 300 tonnes). A picture of a pirate vessel taken in the northern reaches of the Strait of Malacca is shown in Fig. 3.

With these vessels, constraints on position and direction of travel are necessarily much weaker, so the ability of a radar configuration to monitor such traffic must allow for all feasible locations, courses, and speeds. This suggests a figure of merit of the form

$$FoM\_3 = \int_\Omega d\omega \iint_{SoM} w(\boldsymbol{r}) H\left(s(\omega;\boldsymbol{r}) - c(\omega;\boldsymbol{r}) - \varepsilon\right) d\boldsymbol{r} \times \left[\int_\Omega d\omega \iint_{SoM} w(\boldsymbol{r}) d\boldsymbol{r}\right]^{-1} \quad (10)$$

where SoM signifies that the domain of integration is the area constituting the Strait of Malacca. For each of these three figures of merit, the value lies in the interval [0, 1], increasing with the merit of the solution. Two simple options for the function to be minimized are $(1 - FoM)$ and FoM^{-1}.

In the present study, the RCS of the vessel of interest was assigned the constant value 24 dBsm, assumed invariant with azimuth, for a radar operating frequency of 15 MHz. This RCS is representative of a pirate vessel; it is some 30 dB less than that of a large ship such as a tanker. It is a straightforward matter to incorporate frequency- and aspect-dependent scattering behavior given the relevant RCS information.

The figures of merit developed above apply to individual radars, but the essence of the problem under consideration is optimization of a network. The extension to the network case proceeds from the observation that, at any given moment, the target will be detected if at least one radar is able to achieve detection. This can be encapsulated in the following expression:

$$FoM\_4 = \int_L \left[1 - \prod_{j=1}^{n}\left(1 - max_{\omega\in Z} H(s_j(\omega;\boldsymbol{r}) - c_j(\omega;\boldsymbol{r}) - \varepsilon)\right)\right] \times w(\boldsymbol{r})d\boldsymbol{r} \times \left[\int_L w(\boldsymbol{r})d\boldsymbol{r}\right]^{-1}. \quad (11)$$

While this formulation seems reasonable, it does not take into account the advantage of detecting a target with two radars simultaneously, from different directions. Not only is the probability of detection increased but detection-to-track association is improved; this is an important consideration in the dense traffic environment of the Strait of Malacca where ships are on average only ∼5 km apart, not much more than the radar range resolution and less than the azimuthal resolution of the smaller radars. Accordingly, when two radars can view a lane segment, we take dual detectability into account via a performance enhancement factor which is a function of the angle subtended at the target by the two radars.

2) Transverse Current Mapping: Most ships are fitted with GPS, and there are various navigation aids in the Straits of Malacca and Singapore, together with a ship reporting scheme (STRAITREP [19]), but these do not eliminate the risk of accident, particularly where there is scope for human error. The hazards noted earlier make the passage through the Strait of Malacca a challenging undertaking, made even more dangerous at night and during the frequent rain or haze. The dominant southeast to northwest current through the Strait has a typical speed of 1–1.25 knots but, when combined with tidal streams, may reach five knots in some areas [7]. As the flow is perturbed by the shallow, irregular, and time-varying bathymetry, complex mesoscale flows occur, with the potential to divert ships from assigned courses.

For an HF radar system, this suggests a requirement to be able to measure the magnitude of the component of the ocean current perpendicular to the axis of the main shipping lane, $u_\perp(\boldsymbol{r})|_{\boldsymbol{r}\in L}$ with an accuracy better than some specified threshold $u_\perp^{\min}$. Here, we shall adopt the criterion that the lateral displacement of a ship subjected to the transverse current be less than one quarter the separation between north-bound and south-bound lanes when integrated over the time taken for a significant vessel maneuver. The lane separation is typically 2–4 km, though sometimes less, while for a tanker travelling at 16 knots, critical navigation decisions have to be made 20 min in advance. These numbers correspond to a threshold of about 40 cm/s. Thus, to be effective, the radar configuration must be able to resolve to at least this level of precision.

For a current vector $\boldsymbol{u}$, the component $\boldsymbol{u}_\perp$ orthogonal to a shipping lane oriented along the unit vector $\hat{\boldsymbol{e}}$ is given by

$$\boldsymbol{u}_\perp = (\hat{\boldsymbol{e}} \times \boldsymbol{u}) \times \hat{\boldsymbol{e}} \quad (12)$$

which, to the jth monostatic radar, located at $\boldsymbol{r}_j$ and operating at a frequency f, contributes a Doppler shift $\omega_\perp$ given by

$$\omega_\perp \equiv \omega_\perp(\boldsymbol{r}, \boldsymbol{r}_j) = \frac{4\pi f}{c}\boldsymbol{u}_\perp \cdot \hat{\boldsymbol{k}}. \quad (13)$$

Fig. 3. Typical pirate vessel, photographed in the northern reaches of the Strait of Malacca [18].

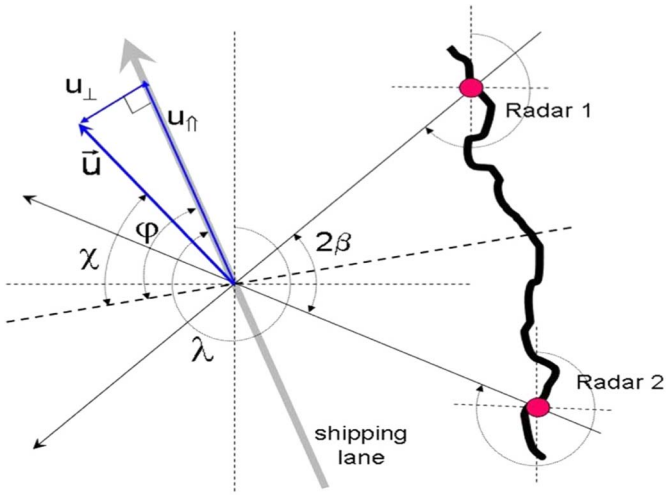

Fig. 4. Radar illumination geometry, showing the transverse current which is the parameter of interest.

Here, $\hat{\boldsymbol{k}}$ is the unit vector aligned with the jth radar look direction

$$\hat{\boldsymbol{k}} = \frac{\boldsymbol{r} - \boldsymbol{r}_j}{|\boldsymbol{r} - \boldsymbol{r}_j|}. \tag{14}$$

Of course, this is not the only current component contributing to the Doppler shift—there is also the portion arising from the current component parallel to the lane, $\boldsymbol{u}_{\Uparrow}$

$$\omega_{\Uparrow} = \frac{4\pi f}{c}\boldsymbol{u}_{\Uparrow} \cdot \hat{\boldsymbol{k}}. \tag{15}$$

The two radar configuration must be able to measure $\boldsymbol{u}_{\perp}$ in the presence of the additive along-lane contribution $\boldsymbol{u}_{\Uparrow}$ which may be up to an order of magnitude greater. This raises some rather subtle complications because of the interaction of waves with currents but for the present we shall ignore these.

The nominal Doppler resolution of each radar is given by $\boldsymbol{\Delta}\omega = 2\pi/T$, where T is the coherent integration time employed by the radar but, allowing for the effects of sampling and signal processing considerations, and the statistical nature of the scattering process, the effective current measurements of the jth radar are only accurate to within some error ε_j. Now, it has been established by comparison with other sensors that overall (vector) current measurement accuracy for radars operating at the upper end of the HF spectrum lies typically in the range $\pm$7–15 cm/s [20], [21]. The nominal accuracy corresponding to the effective Doppler resolution of an individual radar at 25 MHz and integrating for 200s is $\sim$5 cm/s. While this appears more than adequate for our requirement, the combination of radial vectors from two radars to yield a total current vector is plagued by the phenomenon of geometric dilution of precision (GDOP), which can degrade accuracy by an order of magnitude [22]–[24].

The parameters which govern the GDOP for current measurement are 1) the bistatic angle 2β subtended by the two radar axes, and 2) the crossing angle χ, that is the angle between the nominal current direction and the bisector of the two radar axes. These are indicated on Fig. 4. However, in our case, we are interested in the component of the current orthogonal to the lane, shown as $\boldsymbol{u}_{\perp}$, so the relevant crossing angle is φ and the error associated with GDOP must be computed using this angle.

Let the radial component of current velocity derived from a measurement by radar 1 be designated $u_1 + \varepsilon_1$, where ε_1 represents random measurement error, and similarly, that of radar 2 by $u_2 + \varepsilon_2$. The estimates of velocity parallel to and normal to the bisector axis are then given by

$$u_p = \frac{(u_1 + u_2 + \varepsilon_1 + \varepsilon_2)}{2cos\beta} \tag{16}$$

$$u_n = \frac{(u_1 - u_2 + \varepsilon_1 - \varepsilon_2)}{2sin\beta}. \tag{17}$$

We transform this vector measurement into the coordinate system defined by the lane axis and its normal by means of a rotation

$$\begin{bmatrix} u_{\Uparrow} \\ u_{\perp} \end{bmatrix} = \begin{bmatrix} cos\varphi & sin\varphi \\ -sin\varphi & cos\varphi \end{bmatrix} \begin{bmatrix} u_p \\ u_n \end{bmatrix}. \tag{18}$$

Solving for $u_{\perp}$

$$u_{\perp} = \left(\frac{cos\varphi}{2sin\beta} - \frac{sin\varphi}{2cos\beta}\right) u_1 - \left(\frac{cos\varphi}{2sin\beta} + \frac{sin\varphi}{2cos\beta}\right) u_2$$

$$\pm \left[\left(\frac{-sin\varphi}{2cos\beta} + \frac{cos\varphi}{2sin\beta}\right)\varepsilon_1 - \left(\frac{cos\varphi}{2sin\beta} + \frac{sin\varphi}{2cos\beta}\right)\varepsilon_2\right] \tag{19}$$

Assuming ε_1 and ε_2 are independent and identically distributed, the rms error ε is found by squaring and averaging the error term

$$\varepsilon = \frac{\left[cos^2(\varphi + \beta) + cos^2(\varphi - \beta)\right]^{\frac{1}{2}}}{sin\beta}\varepsilon_1. \tag{20}$$

The GDOP is defined as the ratio of the rms error ε to the error ε_1 associated with an individual radar; it is plotted in Fig. 5

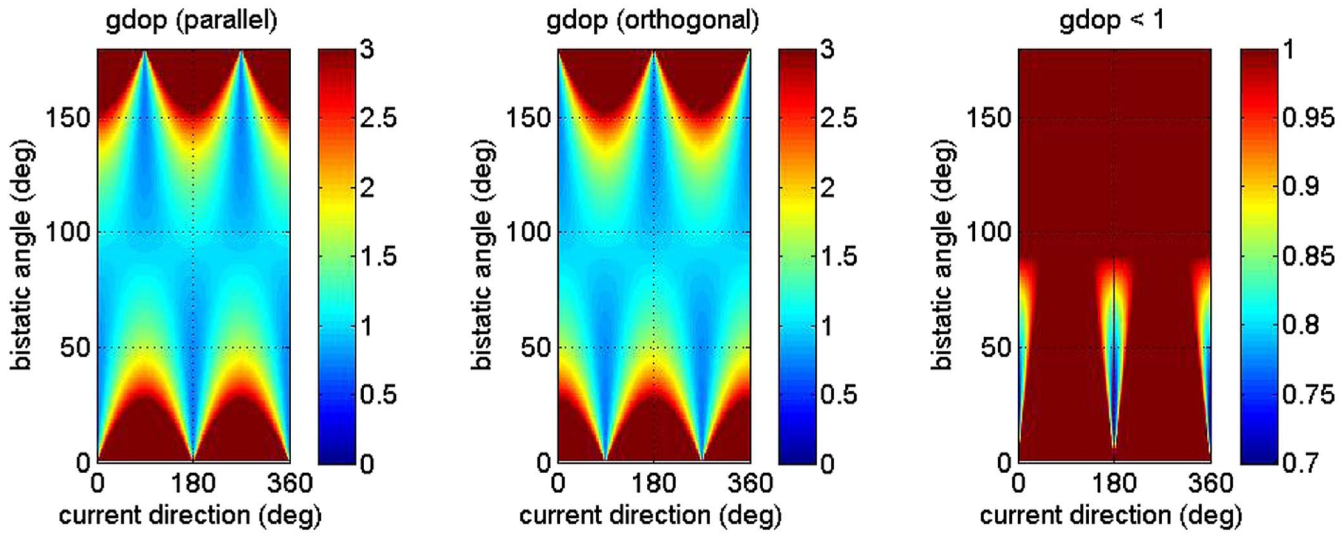

Fig. 5. Dependence of the GDOP factor for current measurements on the bistatic angle of the radar configuration and lane crossing angle. (a) Current component along the lane. (b) Current component orthogonal to the lane. (c) The limited range of geometries for which the two-radar measurement actually reduces the variance of the estimate, i.e., GDOP < 1.

for both parallel and orthogonal components as a function of the bistatic and crossing angles.

From this figure, it is apparent that the geometry has a major bearing on the accuracy of the estimate, more than doubling the errors once the radars depart from orthogonal viewing geometry by more than 50°.

To yield the desired information, the degraded measurement must retain sufficient accuracy to measure transverse current velocities exceeding the threshold value $u_{\perp}^{\min}$. It follows that the integration time is coupled to the observation geometry via the constraint:

$$T > \frac{c \times GDOP}{2f \times \boldsymbol{u}_{\perp}^{min} \cdot \hat{\boldsymbol{k}}}. \tag{21}$$

As the changing environmental conditions impose an upper limit to T, of the order of 10^3 s, this constraint acts as an additional, frequency-dependent spatial filter on effective radar coverage. In the present context with the parameter values used earlier, it limits operational arc extent to $\pm 53^{\circ}$.

3) Visibility and Topographic Constraints: The figures of merit and associated objective functions developed in the preceding sections have made one assumption which demands explicit representation—the spatial integrations have made no allowance for blocking of the signal path from radar to patch of interest by an intervening land mass, either an island or part of the mainland. As it happens, HF surface waves can propagate across land, though with much greater attenuation than across sea, and there is an unusual effect (the Millington effect) through which a considerable fraction of signal strength is restored once the signal reaches the sea beyond the intervening land mass. Nevertheless, unless it cannot be avoided, it is better not to entertain the possibility of exploiting signals which have propagated across one or more islands. We can formalize this constraint on single site acceptability as follows.

Suppose there are K landmasses $\{D_j\}_{j=1,K}$ with coastlines $\{\partial D_j\}_{j=1,K}$ adjoining a sea or ocean of which a region W is to be monitored. From the kth coastline, ∂D_k, construct ∂D_k^+ as follows:

$$\partial \tilde{D}_k^+ = \left\{ \boldsymbol{r} \in \partial D_k \middle| \begin{array}{l} \{\alpha \boldsymbol{r} + (1-\alpha)\boldsymbol{r}'\} \cap D_m = \{0\} \\ \forall \boldsymbol{r}' \in W, \\ \forall m = 1, K; \alpha \in [0,1] \end{array} \right\}. \tag{22}$$

Then, $\partial D_k^+ \subset \partial D_k$ is the subset of the coastline of the kth landmass which has an unobstructed view of the region W. If a radar is to be placed on D_k, then it must lie on ∂D_k^+.

In the present study, where each radar can hope to survey at most a part of the area of concern, it is more appropriate to assign the coverage arc at each candidate radar site and measure the effectiveness of that coverage according to the metrics defined earlier.

Accordingly, we have chosen to define the coverage arcs by the requirement that they exclude any directions which meet regions W for which the site does not belong to ∂D_k^+.

For the present illustrative purposes, we shall not impose other site-specific constraints such as conditions on local topography or coastline orientation and curvature, though these too could be added if desired.

IV. Results

In this section, we present the results of an optimization performed over a selection of 14 sites along the western coast of the Malay peninsula and, optionally, three additional sites on the northern and eastern coasts of Sumatera. When the latter are included, that yields a total of 136 different siting configurations for a two radar system, 680 combinations for a three-radar system, and 2380 for a four-radar system. Analysis of the two radar system has the advantage that a complete evaluation of all possible configurations is computationally feasible and hence can be used as a check on the performance of the genetic algorithm.

TABLE II
LOCATIONS CHOSEN (SOMEWHAT ARBITRARILY) AS CANDIDATE HFSWR SITES TO ILLUSTRATE THE OPTIMIZATION PROCEDURE

SITE	LOCATION	LATITUDE (°N)	LONGITUDE (°E)
1	Pulau Singa Besar	6.195312	099.725283
2	Balik Pulau	5.373210	100.186920
3	Tanjong Piandong	5.056900	100.380500
4	Kuala Gula	4.933300	100.429700
5	Lumut	4.354938	100.577216
6	Sungai Besar	3.649552	101.002744
7	Pulau Ketam	3.030594	101.222771
8	Port Dickson A	2.413153	101.851596
9	Port Dickson B	2.408333	101.857680
10	Melaka	2.151892	102.344980
11	Muar A	1.854671	102.710225
12	Muar B	1.854671	102.710225
13	Batu Pahat	1.756100	102.922200
14	Pulau Kukup	1.325905	103.419840
15	Muara Tiga	5.528300	095.838300
16	Ranto Peureulak	4.863300	097.912500
17	Medan	3.746300	098.763300

The sites employed in this illustrative study are listed in Table II, and marked on the map shown in Fig. 1. They were chosen simply by visual inspection of the coastline as shown in Google Earth, guided by the precept that there should be a more or less uniform sampling of the coastline, supplemented by additional sites offering complementary fields of view, without regard for actual availability for radar deployment or any other detailed considerations such as proximity to electrical power services. The specific domain of integration over which the optimization was carried out is the definition of the Strait of Malacca accepted by the International Hydrographic Organization [25].

Fig. 6(a) shows the set of four solutions obtained from a single run of the genetic algorithm operating on a population of 100 chromosomes, evolved through ten generations as described in Section III-C. At this late stage in the evolution, the set of distinct participating chromosomes has been reduced to only seven members, four of which have satisfied the criterion for Pareto optimality relative to their peers. The fact that each of these solutions is Pareto optimal in a global sense is evident by comparison with Fig. 6(b) which shows the objective space outcomes for the entire set of radar site possibilities. In this universal set, the Pareto front consists of five members, indicated by a distinctive symbol, of which four coincide with those found by the genetic algorithm. In other words, the genetic algorithm has found four of the five optimal solutions. The results of an independent second run of the genetic algorithm are presented in Fig. 7. The outcome is different because random numbers were generated at run-time and used to seed the algorithm and effect the processes of breeding and selection. In this second example, the algorithm is successful in finding all five optimal solutions.

The Pareto optimal solutions correspond to the site combinations {3,3}, {3,5}, {3,6}, {6,6}, and {6,8} as indexed in Table II. It may seem paradoxical that diagonal solutions {3,3} and {6,6} could appear, since a single station cannot estimate total current vector, but these solutions are just a consequence of the fact that we defined the objective function with regard only to transverse current measurement. We include this example specifically to demonstrate the importance of careful definition of the figures of merit and to highlight the non-intuitive nature of multi-objective optimization. In the same vein, it comes as no surprise to discover that, as the maximum effective range of the radars is increased or the coverage arcs are rotated, the set of optimal solutions may change. Thus, for example, with short range radars one finds that it is preferable to reduce overlap, in order to cover more of the shipping lane, provided that the sites chosen have a field of view broadly orthogonal to the lane and are not too distant from it.

Although the power and flexibility of the Pareto front as a guide to site selection in a broader context is obvious, one can envisage situations where a single site recommendation is preferred, as would eventuate under a traditional single-objective ranking criterion. To mimic this in the two-objective environment, we have constructed a scalar figure of merit by taking the product of the figures of merit for ship detection and transverse current estimation. Then, running the genetic algorithm in its single-objective mode, we arrive at the situation summarized in Fig. 8, which shows the distribution of chromosomes and the associated histogram of objective function values for 1) the initial state, 2) an intermediate state, namely, the fourth generation, and 3) the final state, that is, the 10th generation. The convergence is clearly visible and, interestingly, the solution identified happens to be the Pareto optimal solution (3) and (5) identified earlier.

V. DISCUSSION

The results described in the preceding section confirm the applicability of genetic algorithm methodology to the design of HFSWR networks. In this demonstration, the palette of missions was limited to two established radar tasks, but the generality of the approach has the potential to address a much greater diversity of requirements and to focus on very specific applications. For example, the current measurement capability can be adapted to track oil spills, of which about 30 occur on average each year in the Strait of Malacca, and to test the validity of modeling such as that reported in [26]–[28] Many other important applications rely on the ability of HFSWR to estimate the directional wave spectrum. Apart from its more traditional uses, the accurate determination of wave climate at high spatial resolution is essential to support the optimum design and deployment of wave energy converters. This application has direct relevance in the Strait of Malacca context—recent studies [29], [30] have explored the potential of wave energy extraction around Malaysia's coasts, though with an emphasis on the east coast facing the South China Sea. Of course, the technique reported here can just as easily be applied to the South China Sea, where other radar measurement tasks may be relevant.

HFSWR can also contribute to mapping and understanding the properties of the water mass, particularly conductivity properties [31]. The electrical conductivity of Strait of Malacca is strongly influenced by seasonal river outflow and intrusions of high salinity water from the Andaman sea [32], [33]. Moreover, the freshwater flux carries with it various

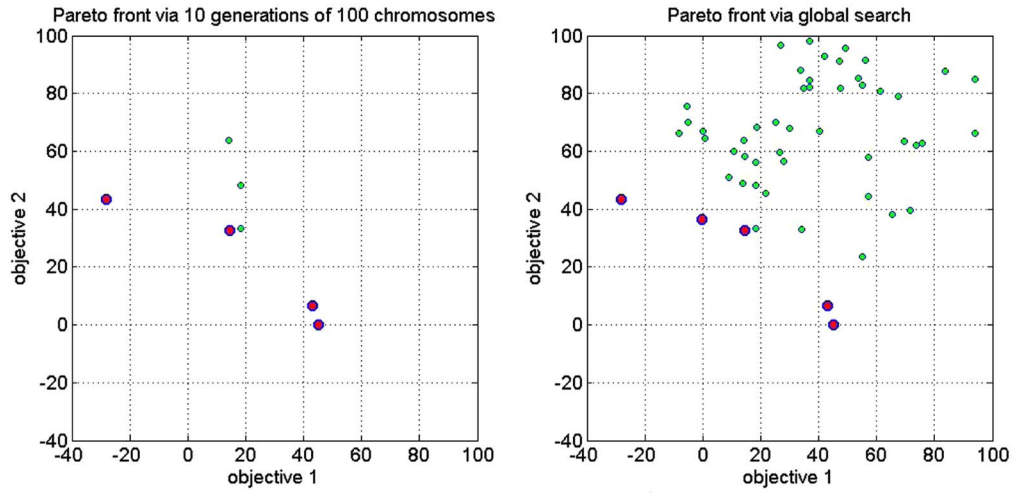

Fig. 6. Objective space comparison of (a) GA-identified solutions, with (b) the set of all possible solutions, generated by exhaustive computation. Objective 1 refers to the ship detection mission, Objective 2 to transverse current measurement. The Pareto dominant solutions are indicated by larger symbols. Run 1.

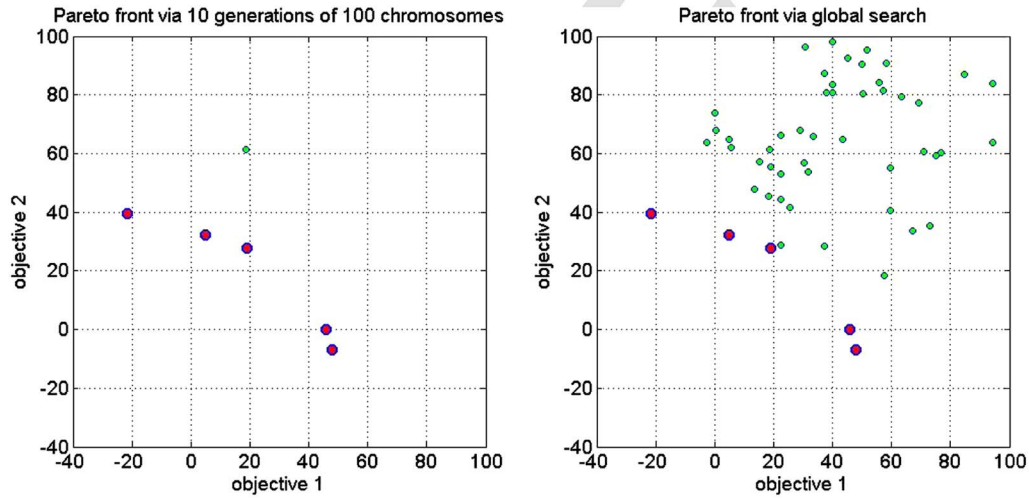

Fig. 7. Objective space comparison of (a) GA-identified solutions, with (b) the set of all possible solutions, generated by exhaustive computation. Run 2. The outcome is different on this second run because different random numbers were generated at run time and used to seed the algorithm and effect the processes of breeding and selection. In this second example, the algorithm is successful in finding all five optimal solutions.

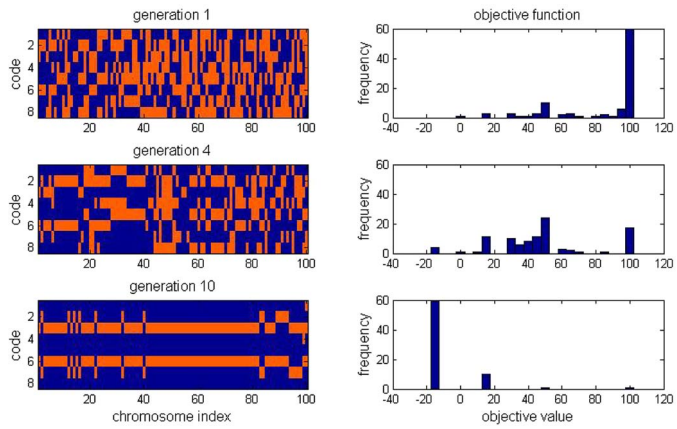

Fig. 8. Evolution of the chromosome population through a number of generations when a single scalar figure of merit is used for ranking. In this picture, the 8-bit genetic codes of the 100 chromosomes which comprise the population are shown (a) at initialization, (b) at the fourth generation, and (3) at the tenth generation. The histograms on the right show the distributions of the corresponding objective function values.

pollutants and organic matter from industries, agriculture, land-reclamation and domestic waste whose distribution has an immediate effect on fish populations [34]. The radar siting optimization problem in this instance is complicated by the desirability of extracting bistatic as well as monostatic scattering signatures.

From the security perspective, the high incidence of piracy in the Strait of Malacca has already been mentioned; to this hazard, we must add the threat from international terrorism which the governments around the strait have identified as a serious prospect. HFSWR is an ideal sensor to detect non-cooperative vessels, either by detecting them directly or by recognizing unorthodox behavior of ships under threat. As HFSWR can monitor wide areas simultaneously, the update time for surveillance of shipping lanes is measured in seconds, not hours [35]. In this mission, the optimization task is extremely complex but all this complexity can potentially be encoded in the objective vector function and used to identify the optimal siting (and other radar design) solutions.

VI. Conclusion

The optimum deployment of a network of HFSWR systems is a highly complex task with many factors to be considered, particularly when the radars are expected to perform multiple roles. Failure to treat the design problem with appropriate care could seriously degrade performance in one or more radar missions.

In this paper, we have described a practical technique for HFSWR network design, based on a genetic algorithm adapted to multi-objective optimization, and demonstrated its efficacy in the context of a hypothetical two-radar system deployed in the Strait of Malacca, a major waterway along which many critical surveillance requirements have been identified. The results confirm that quite disparate criteria can be taken into account with this approach, and support our claim that this methodology can be extended to higher dimensions where exhaustive search is completely out of the question. Of course, in a high dimensional space even the Pareto front may be hard to visualize, but exploratory data analysis techniques such as clustering and dimensionality reduction via compressive sensing may facilitate interpretation.

A key advantage of the Pareto dominance formulation is that it efficiently identifies those solutions which are superior to their fellows according to every criterion tested, and hence greatly reduces the range of design options which need to be considered. The designer is presented with a range of candidate optimal solutions which can be assessed according to additional considerations which may not be meaningfully quantifiable. When we consider domains such as the Strait of Malacca or the South China Sea, where complex geopolitical issues may arise, the virtues of this approach are self-evident.

References

[1] CODAR website. [Online]. Available: http://www.codar.com/

[2] T. Helzel, M. Kniephoff, and L. Pettersen, "Oceanography radar system WERA: Features, accuracy, reliability and limitations," *Turkish J. Elect. Eng. Comput. Sci.*, vol. 18, no. 3, pp. 389–397, 2010.

[3] Helzel Messtechnik website. [Online]. Available: http://www.helzel.com/

[4] S. J. Anderson, P. J. Edwards, P. Marrone, and Y. I. Abramovich, "Investigations with SECAR—A bistatic HF surface wave radar," in *Proc. IEEE Int. Conf. RADAR*, Adelaide, Australia, 2003, pp. 717–722.

[5] S. J. Anderson, "Optimising bistatic HF radar configurations for target and environmental signature discrimination," in *Proc. IDC*, Adelaide, Australia, 2007, pp. 29–33.

[6] B. Tarrant, "Balancing powers in the Malacca Strait," *Reuters News Agency*, Mar. 7, 2010, Accessed Dec. 14, 2011. [Online]. Available: http://blogs.reuters.com/global/2010/03/07/balancing-powers-in-the-malacca-strait/

[7] S. Gran, "MALACCA: The impact of transportation on wildlife in the malacca straits," *Trade Environ. Database Case Studies*, vol. 9, no. 3, p. 573, Sep. 1999, Accessed Dec. 14, 2011.

[8] T. P. Chen, "Prevention measures in the South East Asia region," in *Proc. SPILLCON, Aust. Inst. Petroleum Conf.*, Melbourne, Australia, 2000, Accessed Dec. 14, 2011.

[9] E. Hoffman, *Piracy in Asia: Background report*, Bergen Risk Solutions, Bergen, Norway, Accessed Dec. 14, 2011. [Online]. Available: www.bergenrisksolutions.com/index.php?dokument=569

[10] J. J. Brandon, Reducing piracy in Southeast Asia, Asia Foundation, San Francisco, CA. [Online]. Available: http://asiafoundation.org/in-asia/2009/08/05/reducing-piracy-in-southeast-asia/

[11] International Maritime Bureau, 2011. Accessed Dec. 2011. [Online]. Available: http://www.icc-ccs.org/piracy-reporting-centre/imb-live-piracy-map

[12] B. Hancock, "Singapore raises terror alert on Malacca Strait, one of the world's most important shipping lanes," *Christian Sci. Monitor*, Mar. 5, 2010.

[13] T. M. Sittnick, "State responsibility and maritime terrorism in the Strait of Malacca: Persuading Indonesia and Malaysia to take additional steps to secure the Strait," *Pac. Rim Law Policy J.*, vol. 14, no. 3, pp. 743–769, 2005.

[14] S. J. Anderson, "A parametric wave spectrum model for HF radar applications," Australian Defence Sci. Technol. Org., Edinburgh, SA, Australia, Tech. Rep. DSTO-TR-2727, 2012.

[15] S. J. Anderson, "Optimisation of bistatic HF surface wave radar configurations," in *Proc. IEEE Int. Radar Conf.*, Edinburgh, U.K., pp. 1–4.

[16] D. E. Barrick, "The ocean wave height non-directional spectrum from inversion of the HF sea-echo Doppler spectrum," *Remote Sens. Environ.*, vol. 6, no. 3, pp. 201–227, 1977.

[17] S. J. Anderson and W. C. Anderson, "Bistatic HF scattering from the ocean surface and its application to remote sensing of seastate," in *Proc. IEEE APS Int. Symp.*, Blacksburg, VA, 1987, p. 205.

[18] K. Anderson, *Public Domain Image (Courtesy of US Navy)*, 2006, [Accessed 14 December 2011]. [Online]. Available: http://commons.wikimedia.org/wiki/File:060121-N-5358A-008.jpg

[19] Maritime and Port Authority of Singapore, *Description of STRAITREP*, 2009. Accessed Dec. 14, 2011. [Online]. Available: http://www.mpa.gov.sg/sites/port_and_shipping/port/vessel_traffic_information_system(vtis)/straitrep/description_of_straitrep.page

[20] B. M. Emery, L. Washburn, and J. A. Harlan, "Evaluating radial current measurements from CODAR high-frequency radars with moored current meters," *J. Atmos. Ocean. Technol.*, vol. 21, no. 8, pp. 1259–1271, Aug. 2004.

[21] Y. Yoshikawa, A. Masuda, K. Marubayashi, M. Ishibashi, and A. Okuno, "On the accuracy of HF radar measurement in the Tsushima Strait," *J. Geophys. Res.*, vol. 111, p. C04 009, Apr. 2006.

[22] H. C. Graber, B. K. Haus, R. D. Chapman, and L. K. Shay, "HF radar comparisons with moored estimates of current speed and direction: Expected differences and implications," *J. Geophys. Res.*, vol. 102, no. C8, pp. 18 749–18 766, Aug. 1997.

[23] R. D. Chapman, L. K. Shay, H. C. Graber, J. B. Edson, A. Karachintsev, C. L. Trump, and D. B. Ross, "On the accuracy of HF radar surface current measurements: Inter-comparisons with ship-base sensors," *J. Geophys. Res.*, vol. 102, no. C8, pp. 118 737–18 748, Aug. 1997.

[24] D. A. Trujillo, F. J. Kelly, J. C. Perez, H. R. Riddles, and J. S. Bonner, "Accuracy of surface current velocity measurements obtained from HF radar in Corpus Christi Bay, Texas," in *Proc. IEEE Geosci. Remote Sens. Symp.*, Anchorage, AK, Sep. 2004, pp. 1179–1182.

[25] International Hydrographic Organisation, *Special Publication No. 23* Limits of Oceans and Seas, Monte Carlo, Monaco: Int. Hydrograp. Org. 1953, *Special Publication No. 23*.

[26] M. Marghany, "Modelling of tidal current effects on oil spills movements on Malacca Straits," in *Proc. Asian Conf. Remote Sens.*, Hong Kong, 1999, Accessed Dec. 14, 2011.

[27] S. Rizal, I. Setiawan, T. Iskandar, Y. Ilhamsyah, M. A. Wahid, and M. Musman, "Currents simulation in the malacca straits by using three-dimensional numerical model," *Sains Malaysiana*, vol. 39, no. 4, pp. 519–524, 2010.

[28] H. Assailzadeh, M. Maged, S. B. Mansor, and M. I. Mohamed, "Application of trajectory model, remote sensing and geographic information system (GIS) for oil spill contingency planning in Straits of Malacca," in *Towards Digital Earth—Proc. Int. Symp. Digital Earth*. Marrickville, Australia: Science Press, 1999.

[29] A. M. Muzathik, W. B. Wan Nik, M. Z. Ibrahim, and K. B. Samo, "Wave energy potential of peninsular Malaysia," *ARPN J. Eng. Appl. Sci.*, vol. 5, no. 7, pp. 11–23, Jul. 2010.

[30] A. M. Muzathik, W. B. Wan Nik, K. B. Samo, and M. Z. Ibrahim, "Ocean wave measurements and wave climate prediction of peninsular Malaysia," *J. Phys. Sci.*, vol. 22, no. 1, pp. 77–92, 2011.

[31] R. M. Thomas, "Radio ground wave monitoring of lake salinity," *J. Elect. Electron. Eng., Aust.*, vol. 16, no. 2, pp. 147–153, 1996.

[32] A. M. Amiruddin, Z. Z. Ibrahim, and S. A. Ismail, "Water mass characteristics in the Strait of Malacca using ocean data view," *Res. J. Environ. Sci.*, vol. 5, no. 1, pp. 49–58, 2011.

[33] T. Namba and M. N. Saadon, "Water characteristics of the Malacca Strait and the adjacent sea," in *Proc. IODE-WESTPAC—ICIWP*, Langkawi, Malaysia, Nov. 1–4, 1999, pp. 261–268.

[34] C. K. Tan, J. Ishizaka, S. Matsumura, F. M. Yusoff, and M. I. Mohamed, "Seasonal variability of SeaWifs chlorophyll α in the Malacca Straits in relation to Asian Monsoon," *Continental Shelf Res.*, vol. 26, no. 2, pp. 168–178, Feb. 2006.

[35] S. J. Anderson, B. D. Bates, and M. A. Tyler, "HF surface wave radar and its role in littoral surveillance," *J. Battlefield Technol.*, vol. 2, no. 3, pp. 23–29, Nov. 1999.

Stuart J. Anderson received the B.Sc. and Ph.D. degrees in physics from the University of Western Australia, Perth, Australia, in 1968 and 1972, respectively.

In 1974, he was invited to join the team being assembled in the Australian Defense Science and Technology Organization to develop the Jindalee over-the-horizon radar system, where he assumed responsibility for ocean surveillance and remote sensing. He has worked as a Visiting Scientist in a number of countries, particularly the U.S., U.K., and France, and maintains close links with Curtin University, Perth, as an Adjunct Professor of Applied Physics, with the University of New South Wales, Sydney, Australia, as an Adjunct Professor of Mathematics, with the Université Paris VI, Paris, France, as a Visiting Professor in science and engineering, and as a Professor at the Université Rennes I, Rennes, France which, in 2005, awarded him an honorary doctorate for his contributions to radar science. His interests span ionospheric physics, radiowave propagation, oceanography, electromagnetic scattering, signal processing, passive coherent location, and microwave polarimetry. He has published over 300 journal papers, conference papers, book chapters, and reports in these fields.

Dr. Anderson was the recipient of the 1992 Australian Minister of Defense Award for Research Achievement for his pioneering contributions to over-the-horizon radar in both skywave and surface wave forms.